IEEE Open Journal of
Power Electronics

Received 28 February 2026; accepted 17 March 2026. Date of publication 23 March 2026;
date of current version 8 April 2026. The review of this article was arranged by Associate Editor Alon Kuperman.

Digital Object Identifier 10.1109/OJPEL.2026.3676820

Identification of Interaction Characteristics Between Control and Protection for Co-Design in an MVDC System

JAQUELINE CABAÑAS RAMOS [1], ILKA JAHN [2] (Member, IEEE), FERDINANDA PONCI [3] (Senior Member, IEEE), AND ANTONELLO MONTI [3] (Senior Member, IEEE)

[1]Institute for Automation of Complex Power Systems, RWTH Aachen University, 52074 Aachen, Germany
[2]Division of Electric Power and Energy Systems, KTH Royal Institute of Technology, 100 44 Stockholm, Sweden
[3]Department of Digital Energy, Fraunhofer Institute for Applied Information Technology, 52074 Aachen, Germany

CORRESPONDING AUTHOR: JAQUELINE CABAÑAS RAMOS (e-mail: jaqueline.cabanas@eonerc.rwth-aachen.de)

The work of Jaqueline Cabañas Ramos was supported by the Excellence Strategy of the German Federal Government and the Länder (Junior Principal Investigator Grant at RWTH Aachen). The work of Ilka Jahn was supported by STandUP for Energy.

ABSTRACT Medium-voltage direct current (MVDC) systems exhibit fast fault dynamics and may involve complex interactions between control and protection parameters. This paper applies a global sensitivity analysis (GSA) framework based on Bayesian Sparse Polynomial Chaos Expansion (BSPCE) to an MMC-based MVDC system to, for the first time, quantify both individual and interaction effects of control and protection parameters during pole-to-ground fault scenarios. Results demonstrate for a point-to-point MVDC system, that protection-related parameters — in particular the current-limiting inductor and converter blocking thresholds — are the primary drivers of system behaviour across all studied fault locations. Control parameters exhibit limited direct influence, although minor contributions through interaction effects were observed under certain conditions. While the relative dominance of key protection parameters remains stable across scenarios, the analysis highlights the importance of considering interaction mechanisms, especially when designing system-level protection strategies. Overall, the proposed BSPCE-based GSA approach provides valuable guidance for prioritising key parameters and supports integrated control–protection design in MVDC systems.

INDEX TERMS MVDC, control and protection, global sensitivity analysis, parameter interactions.

I. INTRODUCTION

Medium-voltage direct current (MVDC) distribution systems have gained increasing attention in recent years [1]. According to [2], their adoption is driven by the growing integration of distributed energy resources (DER), the increasing presence of DC loads, and the need for efficient interconnection of power systems. Today, there is even greater interest in applying MVDC technology to electrical grids, as it offers a way to alleviate capacity constraints in aging distribution systems and to support a more sustainable power infrastructure [3].

Despite these advantages, MVDC networks continue to face technical challenges, particularly regarding DC fault management and system design. The lack of mature standards and operational guidelines for MVDC systems highlights the need for further research in this area [3]. DC faults propagate extremely fast due to the absence of natural current zero crossings and the low impedance of DC cables, leading to a rapid fault current rise [4]. The fault current evolution can be divided into three stages: (1) the initial capacitor discharge of the DC link, (2) discharge through the converter freewheeling diodes, and (3) contribution from the AC grid through the converter diodes [5]. In this work, one aim is to assess how pre-fault control design affects the first stage of a pole-to-ground (PTG) fault. Although pole-to-pole (PTP) faults generally result in higher fault currents and are therefore more severe from a thermal and electrical stress perspective, PTG faults are statistically more likely to occur in cable-based MVDC distribution systems [6], [7].

TABLE 1. Comparison of Sensitivity Analysis Approaches for Fault Studies

Method / Paper	Study Focus	Simulation Effort	Robust to Nonlinearities	Interaction Quantification	Suitability for MVDC Fault EMT
Local SA (One-at-a-time) [11]	Converter parameter impact on DC fault behaviour	$\approx k$ per parameter (OAT)	Limited	No	Limited
Screening SA (Morris EE) [12]	DC transients between MMC station and cable	$N_{\text{sim}} = r(k+1)$, $r = 1024 \Rightarrow 2048$ EMT simulations per scenario	Moderate (screening)	Indirect only	Suitable for screening
Screening SA (Morris EE) [13]	MMC parameters impact under AC faults	$N_{\text{sim}} = r(k+1)$, $r = 500 \Rightarrow 4000$ EMT simulations	Moderate (screening)	Indirect only	Suitable for screening
Variance-based global SA (Sobol) [14]	Variance-based full decomposition	$N_{\text{sim}} = N(k+2)$ (thousands for EMT studies)	Yes	Yes (1st and higher order)	High accuracy, high cost
Variance-based global SA (BSPCE-Sobol) [This Work]	PTP MVDC PTG control–protection interaction	$N_{\text{sim}} = N(k+2)$, $N = 20, k = 8 \Rightarrow 360$ simulations per scenario	Yes	Yes (analytical via PCE)	High accuracy, reduced cost

k = number of uncertain input parameters; r = number of Morris trajectories; N = base Monte Carlo sample size for Sobol analysis; N_{sim} = total EMT simulations required per scenario.

For MVDC AC/DC conversion, modular multilevel converters (MMCs) are widely adopted in research due to their high efficiency and scalability [8]. However, MMCs do not provide inherent fault-ride-through (FRT) capability. As a result, the MMC is particularly sensitive to DC faults, making it essential to understand its dynamic response and the parameters that shape it.

Understanding how converter control parameters and protection system behaviour interact during PTG faults is critical for reliable system design. This is especially important because control and protection systems are usually designed separately, and safety requirements dictate that they operate independently [9], which may hide potential coupling effects under fault scenarios.

A. CONTROL AND PROTECTION INTERACTIONS IN DC SYSTEMS

According to [10], high-voltage direct current (HVDC) protection classifies converter behaviour during a DC fault as continuous operation (CO), where MMC blocking is avoided, temporary stop (TS), or permanent stop (PS), where the MMC is blocked. Analysing peak arm currents and blocking thresholds is therefore fundamental, as they determine whether and when converter blocking occurs.

At the system level, the DC circuit breaker (DCCB) must operate fast enough to prevent unnecessary MMC blocking, while the current-limiting inductor must be properly sized to support DCCB operation without adversely affecting converter behaviour. This creates an inherent coupling between device-level dynamics (arm currents and MMC blocking) and system-level protection actions (breaker opening time and current limiting).

Although these considerations are often discussed for multi-terminal systems, analysing a point-to-point configuration provides a worst-case scenario for fault studies and a clear foundation before extending the analysis to multi-terminal MVDC systems. In this context, pre-fault MMC control design—particularly if adjustable by the distribution system operator (DSO)—may influence fault behaviour, affecting both blocking response and arm current magnitudes.

In this study, protection parameters follow hardware design, while the focus is on pre-fault control behavior and system-level interactions. Understanding the combined impact of these elements is essential for assessing control–protection interactions during DC fault events, ensuring that control performance is not compromised.

B. PREVIOUS WORK ON SENSITIVITY ANALYSIS FOR CONTROL AND PROTECTION INTERACTIONS

Table 1 provides a structured overview of the main sensitivity analysis approaches applied to fault studies, including their study focus, computational effort, robustness to nonlinearities, and interaction quantification capabilities.

Different studies have explored the impact of converter control and design on DC fault behaviour. For example, [11] applied a local one-at-a-time sensitivity analysis and showed that converter design significantly affects HVDC protection requirements, highlighting that converter control characteristics, arm inductance, and IGBT ratings strongly influence DC breaker and inductor sizing.

Similarly, [12] used the Morris Elementary Effects screening method and demonstrated in point-to-point configurations that converter properties affect HVDC fault dynamics, with parameters such as blocking delay, active power direction, and arm inductance having a notable impact on peak overcurrent.

[13] also employed the Morris screening technique to identify the most critical MMC control parameters affecting arm stress, AC-side fault current injection, and protection performance under AC faults.

In [8], a variance-based global sensitivity analysis was applied to quantify parameter interactions during pole-to-ground faults for a single MMC, analysing peak DC and arm currents as well as fault current rising time, providing insight into how protection settings interact with converter behaviour. However, the influence of an interconnected MMC and different control modes on control–protection interactions in an MVDC point-to-point configuration remains insufficiently explored.

C. CONTRIBUTION

This work addresses the remaining gaps in quantifying control–protection interactions in MVDC systems. Although existing studies suggest that control settings influence protection behaviour during DC faults, the extent of this influence and the interactions between control and protection parameters remain insufficiently quantified at the system level. This work analyses and quantifies these interactions in a point-to-point MVDC system using global sensitivity analysis (GSA), assessing whether control design is coupled with protection parameters and how this coupling affects protection performance and overall system behaviour during PTG fault scenarios.

The remainder of this paper is organized as follows. Section II describes the sensitivity analysis method. Section IV presents the MVDC case study. Section V reports the sensitivity analysis results, followed by discussion in Section VI. Section VII concludes the paper.

II. SENSITIVITY ANALYSIS

Sensitivity analysis is well established in the literature. However, most studies in the converter control and protection field apply local sensitivity analysis. This work applies global sensitivity analysis for the first time to quantify interactions between control and protection parameters in an MVDC system. The key GSA concepts are briefly recalled here for clarity and to support the understanding of the methodology that is adapted to the specific objectives of this study.

A. VARIANCE-BASED SENSITIVITY ANALYSIS

Variance-based methods are a family of GSA techniques that quantify how much uncertainty in the model output can be attributed to each uncertain input parameter and their interactions [15]. The basic idea is to decompose the variance of the output ($V(Y)$) into contributions from individual inputs ($X_1, \ldots, X_k$) and from combinations of inputs. These contributions are then used to define *Sobol' sensitivity indices*, which are widely used in sensitivity analysis. From this decomposition, the *Sobol' sensitivity indices* are defined:

- *First-order Sobol' indice:*

$$S_i = \frac{V_i}{V(Y)},$$

  where V_i is the contribution of input, and S_i measures the fraction of output variance explained by an input X_i acting alone.
- *Total-effect Sobol' indice:*

$$S_{Ti} = 1 - \frac{V_{\sim i}}{V(Y)},$$

  where $V_{\sim i}$ is the variance of the output when all inputs except X_i are varied. This indice measures the total contribution of X_i, including its interactions with other inputs.

Interpretation is straightforward:

- If S_i is large, X_i has a strong independent effect.
- If $S_{Ti} \gg S_i$, then X_i mainly matters through interactions.
- If both S_i and S_{Ti} are close to zero, X_i can be considered negligible.

B. BAYESIAN SPARSE POLYNOMIAL CHAOS EXPANSION

Variance-based indices can be computed directly from sampling that gives valuable information, but this often requires a very large number of model evaluations: $N(k+2)$ model runs, with k equal to the number of inputs and N could be between a few hundreds to one thousand. To reduce computational cost, the method used in this work applies a surrogate-based approach, namely Bayesian Sparse Polynomial Chaos Expansion (BSPCE) [16]. The central idea is to approximate the model to a surrogate model: instead of running the expensive simulation every time, the polynomial approximation is used.

The BSPCE approach provides measures to describe the surrogate model and how well it represents the original system. **NPCE** indicates the number of polynomial terms used in the approximation, with fewer terms meaning a simpler model. **Vy** is the variance of the output calculated directly from the data, while **VyPCE** is the variance predicted by the surrogate model; if these two values are close, it shows that the surrogate captures the variability of the original system accurately. The **relative training error**, $\varepsilon_{\text{training}}$, quantifies the part of the output variance that the surrogate fails to explain, with smaller values indicating a better fit.

By combining polynomial surrogate modeling with Bayesian sparsity, BSPCE provides an efficient and robust framework for GSA. It reduces the number of required simulations while maintaining accuracy, and the outputs offer a clear and interpretable measure of the surrogate model quality [16].

III. INTERACTION ANALYSIS FRAMEWORK

Before introducing the case study, a structured framework is established to analyse interactions between the control and protection systems. Both subsystems are modelled in

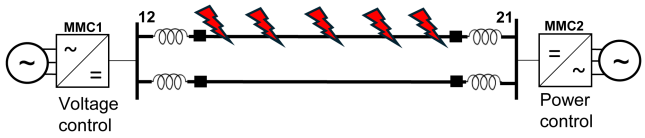

FIGURE 1. MMC-MVDC system.

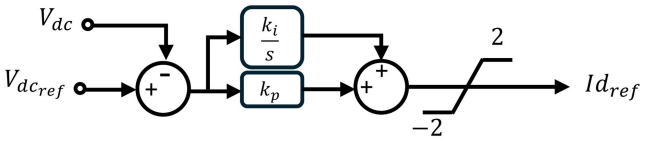

FIGURE 2. DC Voltage control.

TABLE 2. Parameters of the System

Parameter	Value
Rated power	10 MW
Rated AC sec. voltage peak	20.8 kV
DC-side voltage	± 20 kV
Arm impedance	$0.0015 + j0.15$ pu
Number of arm/SMs	36
SM capacitance	40 mF
SCR of Grid	4-20
Line impedance	0.02 Ω/km, 0.75 mH/km

an electromagnetic transient (EMT) simulation using MATLAB/Simulink. EMT simulation captures the non-linear dynamics and enables analysis of PTG fault behaviour in the system. The control system is implemented using discrete PI regulators in block-diagram form: MMC1 regulates the DC voltage, while MMC2 regulates active power.

The protection system is modelled using measurement and logical functions and includes MMC arm overcurrent detection at device level, as well as hybrid DCCB and current-limiting inductor at the system level, supported by primary and secondary line protection algorithms.

In this work, interactions are defined as the combined influence of control and protection design behaviour on the protection response under low-impedance PTG fault conditions. As the objective is to assess system performance for different control and protection configurations, the analysis focuses on the post-fault dynamic behaviour, including transient fault currents and converter blocking actions.

IV. CASE STUDY

A. MVDC SETUP

The case study considers a ±20 kV MVDC point-to-point system, as shown in Fig. 1. The system employs half-bridge MMCs. The cables are modeled using a π-equivalent representation in a symmetrical monopole configuration, each with a length of 10 km.The parameters of the MMCs, DC network and AC grid are presented in Table 2.

The protection system incorporates a hybrid DCCB, modeled as a switch in parallel with a surge arrester, together with a current-limiting inductor. The primary line protection algorithm is based on $\frac{dv}{dt}$ detection, while overcurrent detection serves as a secondary protection method. At the device level, each MMC implements internal overcurrent protection. For the control system, the outer loop control diagram for MMC1 in voltage mode is shown in Fig. 2 and for MMC2 in power mode is shown in Fig. 3

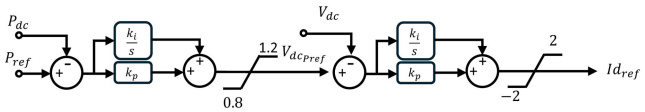

FIGURE 3. Power control [17].

TABLE 3. Control and Protection Input Parameters for BSPCE

Category	Parameter	Lower Bound	Upper Bound
Control parameters	k_p^{VDCreg}	4	8
	k_i^{VDCreg}	100	150
	k_p^{Preg}	0.3	0.9
	k_i^{Preg}	0.1	10
Protection parameters	$\text{BLK}_1^{\text{thr}}$	1.2	2.0
	$\text{BLK}_2^{\text{thr}}$	1.2	2.0
	t_{DCCB} [ms]	0.4	4
	L_{limiter} [H]	1×10^{-6}	70×10^{-3}

B. SCENARIOS AND PARAMETERS UNDER STUDY

1) SCENARIOS

The study considers PTG faults that occur along the cables at 10%, 25%, 50%, 75% and 90% of the cable total length seen from MMC1. PTG faults can be as severe as pole-to-pole faults in a symmetric monopole system, depending on the type of grounding [11]. The selected fault locations are chosen to investigate how the distance between the fault and the converter terminals affects the dynamic interaction between control and protection systems. This also allows assessing whether the interaction between control and protection behaviour depends on the fault position, without pre-assuming any specific trend.

2) INPUT PARAMETERS

The parameters under study, used as inputs for the BSPCE analysis, are summarized in Table 3. The range of control parameters is selected to ensure stable operation across different ranges, while the protection settings are chosen to provide adequate fault response without compromising system stability. Their ranges are validated through stability checks that ensured stable operation for all combinations of parameters.

For the protection parameters, the most critical components are considered in this study. The current-limiting inductor (L_{limiter}) is dimensioned to ensure that fault current rise

TABLE 4. Simulation Outputs Used for BSPCE Analysis

Output Signal	Description
idc_{12}	Peak fault current in line 12
idc_{21}	Peak fault current in line 21
$I_{\text{arm}}^{\text{MMC1}}$	Peak arm fault current in MMC1 during fault
$I_{\text{arm}}^{\text{MMC2}}$	Peak arm fault current in MMC2 during fault
$I_{\text{armBLK}}^{\text{MMC1}}$	Blocking signal for MMC1
$I_{\text{armBLK}}^{\text{MMC2}}$	Blocking signal for MMC2

remains within the defined detection margin and is compatible with the performance characteristics of other protection components. The range of DCCB opening times (t_{DCCB}) is selected according to ideal switching speeds reported in the literature and commercially available devices [18]. The converter overcurrent thresholds are also included and defined by the relation

$$\text{BLK}^{\text{thr}} \cdot i_{\text{peak}} = i_{\text{threshold}},$$

where BLK^{thr} represents an overcurrent safety factor for the power semiconductors of the MMC.

3) OUTPUT PARAMETERS

The outputs analyzed using the BSPCE (Table 4) are the peak DC fault line currents (idc_{12} and idc_{21}), the peak fault arm currents ($I_{\text{arm}}^{\text{MMC1}}$ and $I_{\text{arm}}^{\text{MMC2}}$), and blocking signals ($I_{\text{armBLK}}^{\text{MMC1}}$ and $I_{\text{armBLK}}^{\text{MMC2}}$) of MMC1 and MMC2, all recorded during the initial microseconds and low millisecond range following the PTG fault.

C. BOUNDARY CONDITIONS FOR THE CASE STUDY

Every system is subject to engineering decisions and boundary conditions. To focus on demonstrating the proposed methodology for the identification of parameter interactions, some simplifications are introduced: the system is assumed to remain connected to the AC grid throughout the event (no AC breaker operation), grounding is implemented on the AC side and on the cable of the DC side, the internal control dynamics of the MMC are neglected prioritizing control parameters that may be available to DSO in a multi-terminal multi-vendor system [13], and the cable model is simplified with a π-model.

A π-model is sufficient for the 10 km cable considered [19] and represents a worst-case scenario regarding DC peak overcurrent [20] while avoiding the extra computational cost of a frequency-dependent model. Furthermore, AC grid characteristics (such as short-circuit capacity and Thevenin impedance) and AC breaker dynamics do not significantly influence the initial peak of a DC fault. The initial fault current peak is dominated by the inserted sub-modules capacitor discharge, which occurs over the first14 ms after the fault, and defines the first stage of the fault response. The DCCB operating time lies within this range, whereas the ACCB operating time is typically in the range of $20 - 40$ ms [21]. Thus, only in the later stages — when the DC fault is fed from the AC grid through diodes acting as an uncontrolled rectifier — do the AC grid parameters significantly affect the fault current. At a later stage, the fault current peak and decay depend on the short-circuit capacity of the AC grid, the converter filter impedance, the DC cable impedance, and the fault resistance [5].

In summary, while the above aspects can influence system behavior in practical applications, their exclusion allows for a clear illustration of the proposed methodology for identification of parameter interaction without loss of generality.

TABLE 5. Features of the BSPCE for $I_{\text{arm}}^{\text{MMC1}}$

Feature	Value	Description
NPCE	16.00	Number of elements in the PCE
VyPCE	1088.6	PCE-based estimated variance of $I_{\text{arm}}^{\text{MMC1}}$
Vy	1187.01	Sample variance of $I_{\text{arm}}^{\text{MMC1}}$
$\varepsilon_{training}$	0.1605	Relative training error (% of unexplained variance)

V. RESULTS

To quantify the influence of the control and protection parameters on the outputs in Table 4, the SIML@B BSPCE tool [22] is used, varying the eight input parameters listed in Table 3. An all-at-a-time (AAT) sampling strategy based on a scrambled Sobol sequence ensured uniform and unbiased coverage of the multidimensional parameter space. This approach allows simultaneous variation of all inputs, capturing both direct and interaction effects.

For each sampled parameter set, the detailed Simulink model of the MVDC system is simulated for an 8 s time window, and all outputs are recorded. A total of 360 simulations per fault scenario is selected after testing different sample sizes and simulation settings. With $k = 8$ uncertain inputs, this corresponds to $N/k = 45$, which is substantially higher than the commonly adopted practical guideline of $N \approx 10\text{–}20 \times k$ for PCE-based surrogate construction [23]. The simulations are executed on an 11th-Gen Intel(R) Core(TM) i5-1145G7 @ 2.60 GHz computer and require approximately 6 hours per scenario. For comparison, a traditional variance-based GSA would require $N(k + 2)$ simulations. With $k = 8$ inputs and a conservative $N = 500$, this yields $500 \times (8 + 2) = 5000$, corresponding to approximately 83 hours per scenario on the same hardware.

The simulation results are exported in CSV format and analysed in SIML@B to compute the first-order (S_i) and total (S_T) Sobol indices for each output. The reliability of these indices depends on the accuracy of the BSPCE surrogate model. Table 5 summarises the main diagnostic metrics. For example, for $I_{\text{arm}}^{\text{MMC1}}$ under a 10% PTG fault, the NPCE value of 16 indicates that sixteen polynomial terms are selected as the optimal basis. The PCE-based variance estimate ($V_y^{\text{PCE}} = 1088.6$) closely matches the sample variance from the simulation data ($V_y = 1187.01$), indicating stable variance representation. The relative training error of $\varepsilon_{\text{training}} = 0.16$

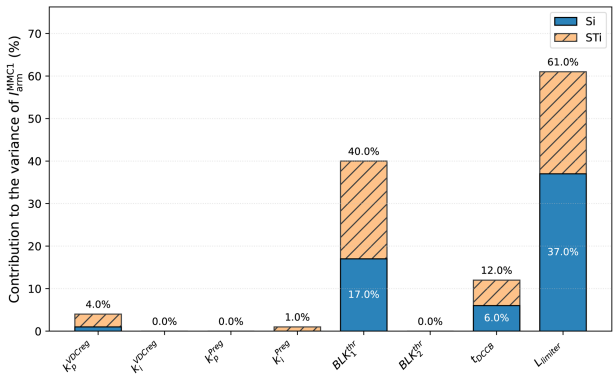

FIGURE 4. Scenario 1: Direct (S_i) and total (S_T) Sobol indices for the arm current of MMC1.

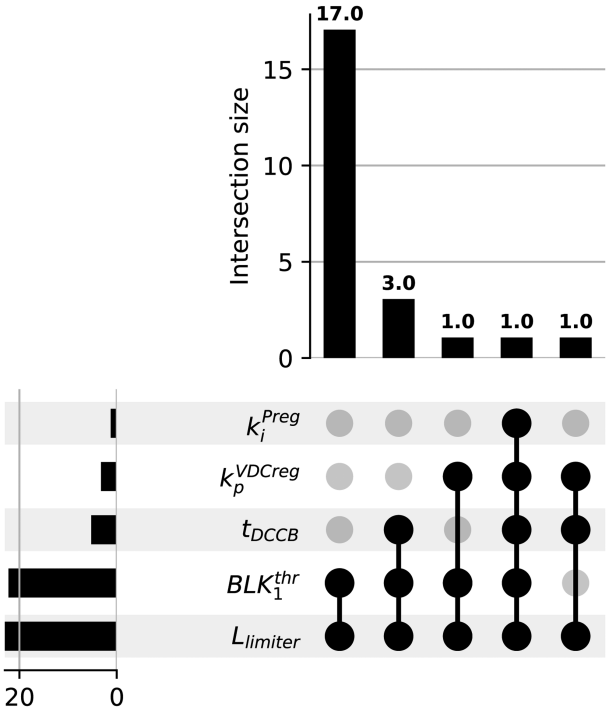

FIGURE 5. Scenario 1: Parameter interaction contributions for the arm current of MMC1.

corresponds to a coefficient of determination of approximately $R^2 \approx 0.84$, meaning that the surrogate explains about 84% of the output variance.

Given this level of accuracy and the sparse polynomial structure, the surrogate model is considered sufficiently reliable for variance-based sensitivity ranking within the bounded input domain used for sampling [16]. No extrapolative predictions outside this domain are performed or claimed in this study. While very small interaction effects may fall within the approximation error margin, the main conclusions rely on dominant first- and total-order indices, which exhibit substantially larger magnitudes. Accordingly, low-magnitude interaction terms are interpreted conservatively and are not overemphasized in the discussion.

The BSPCE results are presented in bar figures showing the first-order and total Sobol indices for an output, along with separate interaction plots among inputs. As described in Section IV, the same set of inputs and outputs is analysed for each scenario. Due to space constraints, the following subsections present three representative fault locations (10%, 50%, and 90% of the line) and focus on one illustrative output from Table 4: the arm fault current of MMC1, $I_{\text{arm}}^{\text{MMC1}}$.

A. SCENARIO 1: FAULT AT 10% OF THE LINE LENGTH

Fig. 4 presents the direct (S_i) and total (S_T) Sobol indices obtained for $I_{\text{arm}}^{\text{MMC1}}$,including their associated Bayesian uncertainty bounds (ΔS_i, ΔS_{T_i}) provided by the BSPCE framework.

The current-limiting inductor (L_{limiter}) is the most influential parameter in this fault scenario,with $S_i = 0.37 \pm 0.05$ and $S_T = 0.61 \pm 0.04$. Since $S_i \neq S_T$, this indicates that L_{limiter} alone contributes 37% to the variance of $I_{\text{arm}}^{\text{MMC1}}$, with interaction effects increasing this contribution to 61%. Importantly, the magnitude of these indices is significantly larger than their associated uncertainty bounds, confirming their statistical robustness.

The next most relevant parameter is the overcurrent safety threshold of MMC1 ($\text{BLK}_1^{\text{thr}}$), with $S_i = 0.17 \pm 0.03$ and $S_T = 0.40 \pm 0.04$. These values remain well separated from zero relative to their uncertainty, indicating a clearly identifiable influence.

Additionally, the circuit breaker opening time (t_{DCCB}) plays a smaller role, with $S_i = 0.06 \pm 0.02$ and $S_T = 0.12 \pm 0.03$, indicating partial contribution through interactions. The effect of the DC voltage controller proportional gain (k_p^{VDCreg}) is minimal, with a total contribution of $S_T = 0.04 \pm 0.02$, and only through interaction effects.

The BSPCE results also provide insight into parameter interactions. In Fig. 5, the vertical bars (labelled *intersection size*) represent the magnitude of each specific interaction between input parameters, showing their exact contribution to the variability of the output. For example, L_{limiter} and $\text{BLK}_1^{\text{thr}}$together produce the 17% of the variability of $I_{\text{arm}}^{\text{MMC1}}$. The horizontal bars indicate the total contribution of each individual parameter, summing all interactions in which that parameter is involved. In this case, interactions primarily involve $\text{BLK}_1^{\text{thr}}$ and L_{limiter}, (both above 20% on horizontal bar) indicating that these protection parameters tend to act jointly with many inputs in influencing the variance of $I_{\text{arm}}^{\text{MMC1}}$.

Finally, the BSPCE results indicate which parameters have a negligible influence on this output. For $I_{\text{arm}}^{\text{MMC1}}$, the proportional and integral gains of the power regulator (k_p^{Preg}, k_i^{Preg}), the integral gain of the voltage regulator (k_i^{VDCreg}), and the overcurrent safety factor of MMC2 ($\text{BLK}_2^{\text{thr}}$) can be considered insignificant in this scenario.

B. SCENARIO 2: FAULT AT 50% OF THE LINE LENGTH

Following the same approach as in the previous subsection, this subsection presents the BSPCE results for the arm fault

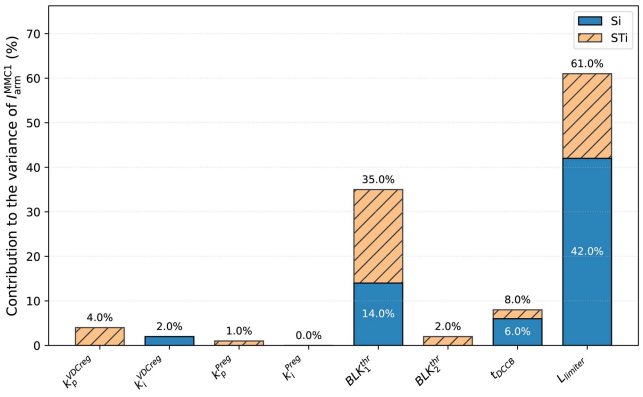

FIGURE 6. Scenario 2: Direct (S_i) and total (S_T) Sobol indices for the arm current of MMC1.

current of MMC1 ($I_{\text{arm}}^{\text{MMC1}}$). As shown in Fig. 6, the current-limiting inductor (L_{limiter}) remains the dominant contributor to the variance of $I_{\text{arm}}^{\text{MMC1}}$, with $S_i = 0.42 \pm 0.04$ and $S_T = 0.61 \pm 0.04$, indicating both strong direct influence and significant interaction effects. The overcurrent safety threshold of MMC1 ($\text{BLK}_1^{\text{thr}}$) is the second most influential parameter, with $S_i = 0.14 \pm 0.03$ and $S_T = 0.35 \pm 0.03$, also showing notable interactions with other inputs. The opening time of the DC circuit breaker (t_{DCCB}) has a smaller but still measurable influence, with $S_i = 0.06 \pm 0.02$ and $S_T = 0.08 \pm 0.02$, indicating moderate interaction effects.

Regarding the control parameters, both the proportional and integral gains of the power regulator (k_p^{Preg}, k_i^{Preg}) exhibit negligible influence, with indices close to zero and comparable to their uncertainty bounds. The DC voltage regulator gains show limited impact: k_p^{VDCreg} appears only through interactions ($S_T = 0.04 \pm 0.02$), while k_i^{VDCreg} contributes marginally ($S_i = 0.02 \pm 0.01$). Parameters whose sensitivity indices are of the same order as their uncertainty are considered statistically insignificant and are therefore not overinterpreted.

Parameter interactions are illustrated in Fig. 7. In this case, the interaction between L_{limiter} and $\text{BLK}_1^{\text{thr}}$ contributes 18% to the variance of $I_{\text{arm}}^{\text{MMC1}}$. Smaller interaction effects are also observed between $\text{BLK}_1^{\text{thr}}$ and k_p^{VDCreg}, and between $\text{BLK}_1^{\text{thr}}$ and t_{DCCB}, each contributing approximately 2% to the variance of $I_{\text{arm}}^{\text{MMC1}}$.

Overall, the BSPCE results for this scenario confirm that k_i^{VDCreg}, k_p^{Preg}, k_i^{Preg}, and $\text{BLK}_2^{\text{thr}}$ have minimal impact on $I_{\text{arm}}^{\text{MMC1}}$ and can therefore be excluded from further analysis in this context.

C. SCENARIO 3: FAULT AT 90% OF THE LINE LENGTH

For the case of a fault occurring at 90% of the line length from MMC1, the BSPCE results shown in Fig. 8, confirm that the current-limiting inductor (L_{limiter}) remains the dominant contributor to the variance of $I_{\text{arm}}^{\text{MMC1}}$, with $S_i = 0.30 \pm 0.05$ and $S_T = 0.58 \pm 0.05$, indicating both strong direct influence and significant interaction effects. The overcurrent

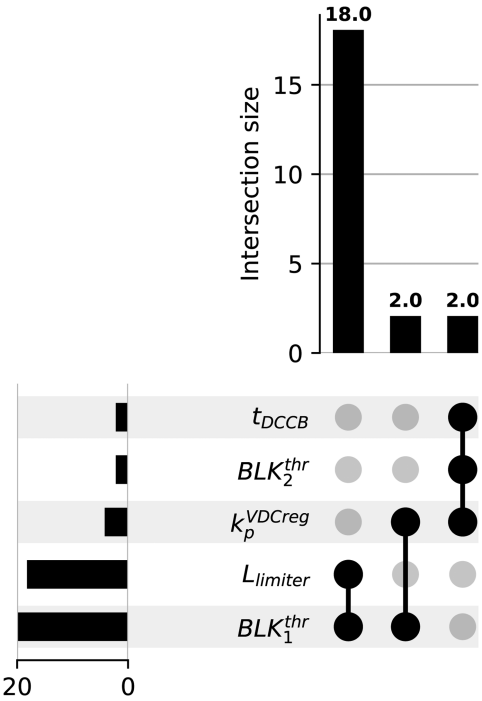

FIGURE 7. Scenario 2: Input interactions for the arm current of MMC1.

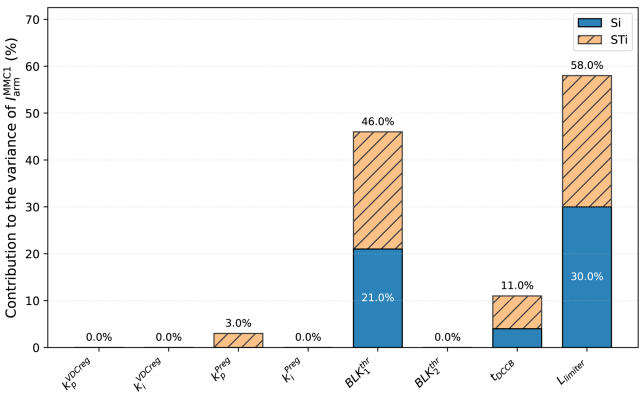

FIGURE 8. Scenario 3: Direct (S_i) and total (S_T) Sobol indices of the arm current of MMC1.

safety threshold of MMC1 ($\text{BLK}_1^{\text{thr}}$) is the second most influential parameter, with $S_i = 0.21 \pm 0.04$ and $S_T = 0.46 \pm 0.05$, also showing notable interactions with other inputs. The opening time of the DC circuit breaker (t_{DCCB}) has a smaller influence, with $S_i = 0.04 \pm 0.02$ and $S_T = 0.11 \pm 0.03$, indicating moderate interaction effects.

Regarding the control parameters, only the proportional gain of the power regulator (k_p^{Preg}) exhibits a very small impact, contributing exclusively through interactions ($S_T = 0.03 \pm 0.02$) and can be discarded, as can the remaining control gains (k_i^{Preg}, k_p^{VDCreg}, k_i^{VDCreg}) that have negligible influence.

The interaction contributions are illustrated in Fig. 9; similar to the other scenarios, the combination of L_{limiter} and

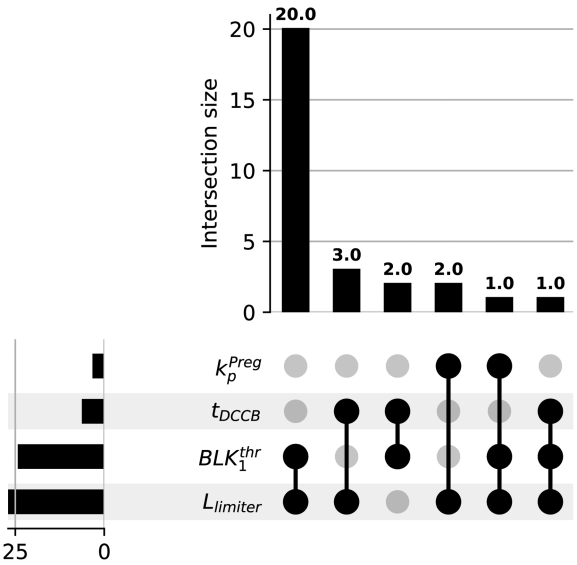

FIGURE 9. Scenario 3: Input interactions for the arm current of MMC1.

$\mathrm{BLK}_1^{\mathrm{thr}}$ produces the largest interaction effect, accounting for 20% of the total variance of $I_{\mathrm{arm}}^{\mathrm{MMC1}}$. Other interactions involving t_{DCCB} and k_p^{Preg} are also present but contribute only marginally.

For this output and fault location, all parameters except L_{limiter}, $\mathrm{BLK}_1^{\mathrm{thr}}$, t_{DCCB}, and k_p^{Preg} can be excluded from further detailed analysis.

D. COMBINED SCENARIOS

In this subsection, the results from the 25% and 75% fault locations are incorporated to determine whether simulations can be limited to three extreme cases (e.g., 10%, 50%, 90%), or if intermediate fault positions must also be considered. The aggregated BSPCE results from the five scenarios, covering all outputs listed in Table 4, are summarized in Figs. 10 and 11. Fig. 10 presents the total Sobol indices (S_T) for each output across all fault locations.

For the peak arm fault current $I_{\mathrm{arm}}^{\mathrm{MMC1}}$, the impact of L_{limiter}, $\mathrm{BLK}_1^{\mathrm{thr}}$ and t_{DCCB} varies with fault location. At 10%, 50% and 90% of the line, L_{limiter} contributes approximately 60% of the variance, while this influence reduces to around 40% at 25% and 75% line length. The parameters $\mathrm{BLK}_1^{\mathrm{thr}}$ and t_{DCCB} show a relatively consistent effect, independent of the fault distance. Control parameters exhibit consistently small contributions. Similar trends are observed for the peak arm fault current $I_{\mathrm{arm}}^{\mathrm{MMC2}}$, where the influence of $\mathrm{BLK}_2^{\mathrm{thr}}$, t_{DCCB} and L_{limiter} depends on the distance, with $\mathrm{BLK}_2^{\mathrm{thr}}$ ranging from approximately 40% at 90% of the line to 60% at 10%. The effect of L_{limiter} increases closer to MMC2. Again, control parameters present only minor contributions to the overall variance.

The blocking signal $I_{\mathrm{armBLK}}^{\mathrm{MMC1}}$ and $I_{\mathrm{armBLK}}^{\mathrm{MMC2}}$ are consistently dominated by the protection-related parameters t_{DCCB}, $\mathrm{BLK}_1^{\mathrm{thr}}$, $\mathrm{BLK}_2^{\mathrm{thr}}$ and the current-limiting inductance L_{limiter}. Although minor changes are observed depending on the fault location, the relative influence of the dominant parameters remains stable. Control parameters show a negligible impact in isolation, suggesting that pre-fault controller configuration does not significantly affect converter blocking in the current two-terminal configuration.

For peak fault currents in the line i_{dc12} and i_{dc21}, Fig. 10 shows that the sensitivity levels of L_{limiter}, $\mathrm{BLK}_1^{\mathrm{thr}}$, $\mathrm{BLK}_2^{\mathrm{thr}}$ and t_{DCCB} are similar across all distances. This reveals that the impact of these protection parameters on the variability of the peak DC fault current dynamics is independent of the fault location, with no significant increase in interaction between control and protection parameters. As in the previous outputs, the contributions from control parameters remain negligible.

Interaction results in Fig. 11 further highlight that L_{limiter} has the strongest cumulative interaction effects, exceeding 250% on the horizontal bar, followed by $\mathrm{BLK}_1^{\mathrm{thr}}$ and $\mathrm{BLK}_2^{\mathrm{thr}}$. The most significant pairwise interaction occurs between L_{limiter} and $\mathrm{BLK}_1^{\mathrm{thr}}$ responsible for 198% of the variance of the different analyzed outputs, followed by the interaction between L_{limiter} and $\mathrm{BLK}_2^{\mathrm{thr}}$ with a total sum of 148%. The interaction between L_{limiter} and t_{DCCB} contributes 36%.

These values are obtained by summing the second- and higher-order Sobol' indices across all outputs and fault locations. Hence, the reported percentages represent cumulative interaction contributions rather than averages, maintaining the variance-based structure of the Sobol' decomposition and revealing globally dominant effects.

Although control parameters show limited influence in isolation, it is noteworthy that some interaction effects are detected, with specific cases showing up to 9% contribution through parameter interaction.

VI. DISCUSSION

The sensitivity analysis across six outputs, eight input parameters, and five fault locations shows that PTG fault behaviour is governed primarily by protection-related parameters. The total Sobol indices (S_T) consistently identify $\mathrm{BLK}_1^{\mathrm{thr}}$, $\mathrm{BLK}_2^{\mathrm{thr}}$, t_{DCCB}, and L_{limiter} as the dominant drivers of output variance, while control parameters contribute only marginally. Although numerical values change with fault position, the hierarchy of the main protection parameters' impact is stable.

Fig. 10 highlights clear control mode-dependent trends; for MMC1, operating in DC voltage control, the current-limiting inductor L_{limiter} dominates the variance of both the peak arm fault current ($I_{\mathrm{arm}}^{\mathrm{MMC1}}$) and the blocking signal ($I_{\mathrm{armBLK}}^{\mathrm{MMC1}}$). In contrast, for MMC2 in power-control mode, the overcurrent safety factor $\mathrm{BLK}_2^{\mathrm{thr}}$ is the most influential parameter for $I_{\mathrm{arm}}^{\mathrm{MMC2}}$ and $I_{\mathrm{armBLK}}^{\mathrm{MMC2}}$. This indicates that the inductor mainly affects the converter that regulates DC voltage, while blocking thresholds play a stronger role in power-controlled operation. In addition, Fig. 11 reinforces the central influence of L_{limiter}, which consistently shapes transient behaviour across different scenarios.

Although control parameters exhibit low first-order effects, non-negligible interaction contributions appear in some

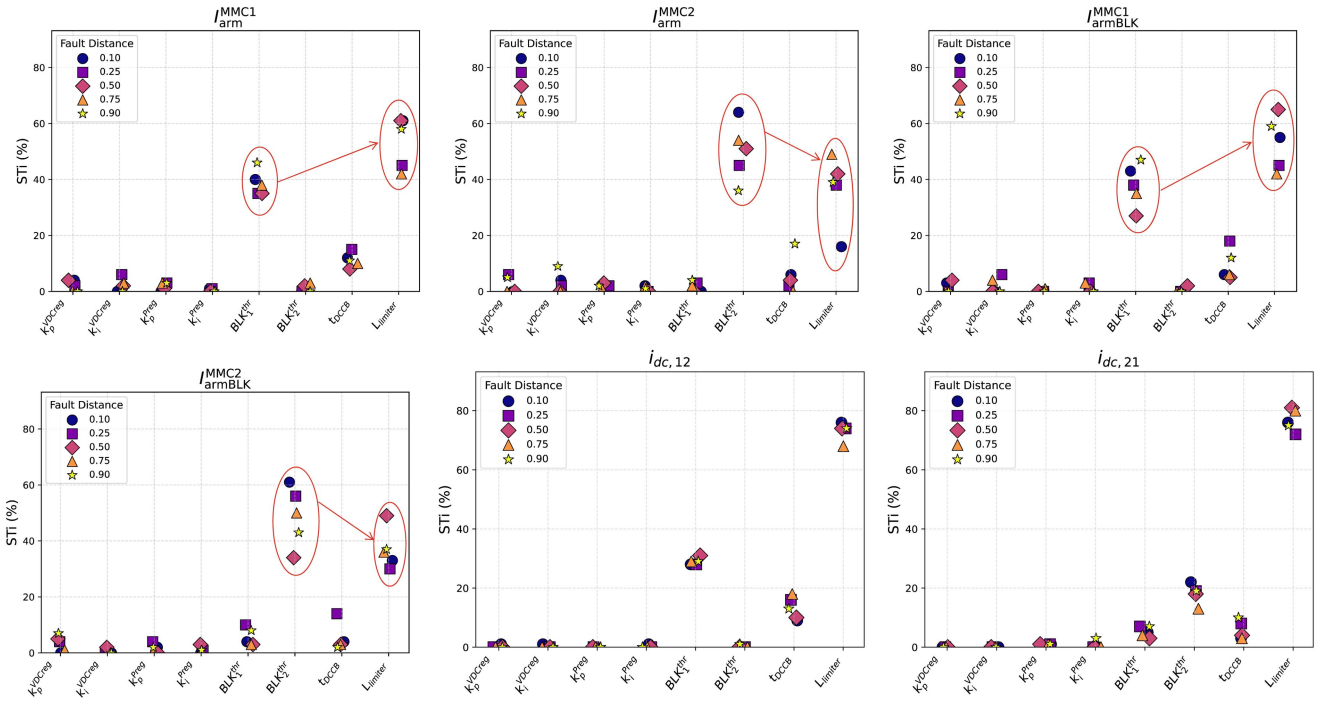

FIGURE 10. Global Sobol Total-Effect indices ST_i for the six monitored outputs under all fault-distance scenarios.

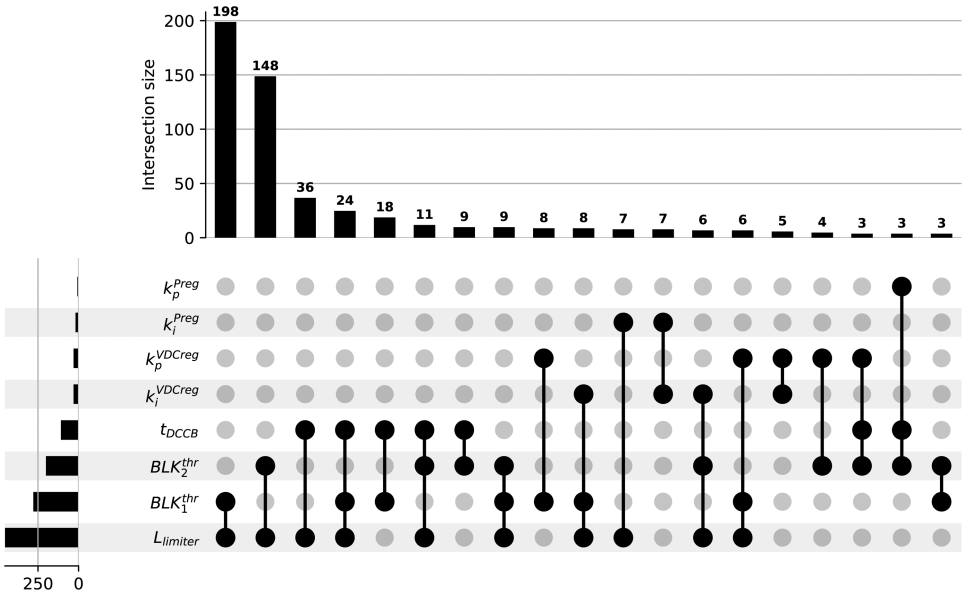

FIGURE 11. Global interaction contributions across all fault distances.

cases, which remain secondary to the dominant protection-related parameters. These interactions indicate that, even when considering outer-loop control only, certain settings may influence protection performance when combined with key protection parameters.

From a design perspective, the results establish a clear hierarchy for parameter selection. The dominant interaction contribution of L_{limiter} suggests that its sizing fundamentally shapes fault current dynamics and should therefore be prioritised in the design process. Subsequently, converter blocking thresholds and breaker operating times can be tuned to ensure coordinated and robust protection performance.

While control parameters remain secondary in the investigated two-terminal configuration, their influence may increase in multi-terminal MVDC grids, where stronger converter coupling enhances control–protection interdependence. The

proposed sensitivity analysis framework is directly applicable to such configurations without methodological modification.

These findings underline the benefit of system-level assessment. Even when individual control and protection strategies appear adequate, their combined dynamics during faults can lead to behaviors that are not captured analytically. Global sensitivity analysis provides a systematic means of identifying these coupled effects and guiding parameter prioritisation.

Finally, the methodology presented here is broadly applicable to other domains where complex systems combine traditionally separate aspects, such as coordinated control and protection, multi-converter operation, or integrated energy systems. By efficiently quantifying both individual parameter effects and interactions, this approach can inform design decisions in systems where analytical derivation of interactions is impractical.

VII. CONCLUSION

A global sensitivity analysis is conducted to investigate control–protection parameter interactions for pole-to-ground faults in a point-to-point MMC-MVDC system using a Bayesian Sparse Polynomial Chaos Expansion method. This approach enables reliable sensitivity estimation with only 360 simulations per scenario instead of the 5000 required by a traditional variance-based GSA, reducing the computational effort from approximately 83 hours to 6 hours per scenario (an 85% reduction).

Five fault scenarios located at 10%, 25%, 50%, 75%, and 90% of the cable length from MMC1 are analysed, considering outputs such as peak DC fault line currents, arm currents, and converter blocking signals. The BSPCE results indicate that considering extreme cases may be sufficient to obtain reliable ranking information of the main parameters affecting output variance.

The results also show that the current-limiting inductor (L_{limiter}) and the overcurrent safety factors ($\text{BLK}_1^{\text{thr}}$, $\text{BLK}_2^{\text{thr}}$) are the most influential parameters across all scenarios. Among the control parameters, the proportional and integral gains of the DC voltage controller (k_p^{VDCreg}, k_i^{VDCreg}) exhibit minor influence and only through interaction effects.

Strong interaction contributions are observed, particularly involving L_{limiter}, $\text{BLK}_1^{\text{thr}}$, and $\text{BLK}_2^{\text{thr}}$, identifying these as the most critical design parameters. These findings support prioritising their tuning early in the design process to minimise the need for re-adaptation of other control and protection functions. Although the analysis confirms only a limited impact of control settings in a point-to-point configuration, the observed interaction through k_p^{VDCreg} and k_i^{VDCreg} suggests that control–protection coupling may become more significant in more complex architectures, such as multi-terminal MVDC systems.

Overall, this study demonstrates the applicability of BSPCE-based GSA to identify key interdependencies in MVDC fault dynamics and supports a more integrated and robust converter and protection design methodology.

REFERENCES

[1] CIGRE Working Group C6.31, "Medium voltage DC distribution systems," CIGRE, Tech. Brochure 875, 2022. [Online]. Available: https://www.e-cigre.org/publications/detail/875-medium-voltage-dc-distribution-systems.html

[2] CIGRE, " Medium voltage direct current (MVDC) grid feasibility study," 2020. [Online]. Available: https://electra.cigre.org/309-april-2020/technical-brochures/medium-voltage-direct-current-mvdc-grid-feasibility-study.html

[3] "Iec white paper: MVDC grids–medium voltage DC (MVDC) grids for an all-electric society," Int. Electrotech. Commission, Geneva, Switzerland, White Paper 109247, 2025. [Online]. Available: https://webstore.iec.ch/en/publication/109247

[4] A. Kaharević, J. C. Ramos, I. Jahn, F. Ponci, and A. Monti, "A review of HVDC and MVDC grid protection," in *Proc. IET Conf. Proc.*, 2023, vol. 2023, pp. 271–280.

[5] K. Sharifabadi, L. Harnefors, H. P. Nee, S. Norrga, and R. Teodorescu, "Design, control and application of modular multilevel converters for hvdc transmission systems," in *Design, Control and Application of Modular Multilevel Converters for HVDC Transmission Systems*. Hoboken, NJ, USA: Wiley, Sep. 2016, pp. 1–386, doi: 10.1002/9781118851555.

[6] Y. Xu et al., "A practical pole-to-ground fault current calculation method for symmetrical monopole DC grids," *Electronics*, vol. 13, 2024, Art. no. 4245, doi: 10.3390/electronics13214245.

[7] A. Kaharevic, F. Ponci, and A. Monti, "Impact of system parameters on selectivity requirements for MVDC grids," in *Proc. 2025 IEEE 7th Int. Conf. DC Microgrids*, 2025, pp. 1–25.

[8] J. C. Ramos, I. Jahn, F. Ponci, and A. Monti, "DC-side interaction studies for control and protection in an MVDC system," in *Proc. IEEE 7th Int. Conf. DC Microgrids*, 2025, pp. 1–5.

[9] "Protection & control for HVDC systems: Technical specification ts3.24.90 (res) – issue 1, october 2014," Nat. Grid Electricity Transmiss. PLC, London, U.K., Tech. Specification TS3.24.90 (RES), Oct. 2014, uncontrolled When Printed. [Online]. Available: https://www.neso.energy/document/33201/download

[10] International Electrotechnical Commission, "High voltage direct current (HVDC) grid systems and connected converter stations–guideline and parameter lists for functional specifications: Part 1: Guideline," Int. Electrotech. Commission, Geneva, Switzerland, Tech. Specification IEC TS 63291-1, Sep. 2023. [Online]. Available: https://webstore.iec.ch/en/publication/65825

[11] P. Düllmann, C. Brantl, C. Klein, and A. Moser, "Interdependencies in HVDC grid protection: Impact of converter parameters and controls on dc fault-ride-through capabilities and protection system design," *IET Gener., Transmiss. Distrib.*, vol. 17, pp. 2356–2375, May 2023.

[12] H. Saad, P. Rault, M. Goertz, and S. Wenig, "Parameter sensitivity analysis on dc transients between mmc station and cable," *Electric Power Syst. Res.*, vol. 196, 2021, Art. no. 107277. [Online]. Available: https://www.sciencedirect.com/science/article/pii/S0378779621002583

[13] X. Liu, W. Leterme, P. D. Judge, G. C. Chaffey, and D. Van Hertem, "Identification of critical parameters for AC fault response of modular multilevel converters with partially black-boxed control," *IEEE Trans. Power Del.*, vol. 40, no. 6, pp. 3031–3046, Dec. 2025.

[14] M. Ginocchi, F. Ponci, and A. Monti, "Sensitivity analysis and power systems: Can we bridge the gap? A review and a guide to getting started," *Energies*, vol. 14, no. 24, 2021, Art. no. 8274. [Online]. Available: https://www.mdpi.com/1996-1073/14/24/8274/htm

[15] A. Saltelli et al., *Global Sensitivity Analysis: The Primer*. Chichester, U.K.: Wiley, 2008.

[16] Q. Shao, A. Younes, M. Fahs, and T. A. Mara, "Bayesian sparse polynomial chaos expansion for global sensitivity analysis," *Comput. Methods Appl. Mechan. Eng.*, vol. 318, pp. 474–496, 2017. [Online]. Available: https://www.sciencedirect.com/science/article/pii/S0045782516307010

[17] W. Lin, D. Jovcic, S. Nguefeu, and H. Saad, "Coordination of MMC converter protection and DC line protection in DC grids," in *Proc. IEEE Power Energy Soc. Gen. Meeting*, Nov. 2016, pp. 1–5.

[18] "Long-term view for HVDC technology: Whitepaper WG4 (deliverable 4.4)," READY4DC Project (Horizon Europe), Aachen, Germany, Whitepaper/Tech. Rep. Deliverable 4.4, Nov. 2023. [Online]. Available: https://www.ready4dc.eu
[19] J. Yang, J. O'Reilly, and J. E. Fletcher, "An overview of DC cable modelling for fault analysis of VSC-HVDC transmission systems," in *Proc. 20th Australas. Universities Power Eng. Conf.*, Christchurch, New Zealand, 2010, pp. 1–6.
[20] A. Mouhaidali, S. Marache, P. Dworakowski, M. Henriksen, and L. Dalmar, "Impact of cable modeling in electromagnetic transient simulations of MVDC systems," 2023. [Online]. Available: https://hal.science/hal-04163562v1
[21] "Broad comparison of fault clearing strategies for DC grids," PROMOTioN Project (Horizon 2020), Brussels, Belgium, Tech. Rep. Deliverable D4.2, Mar. 2020. [Online]. Available: http://www.promotion-offshore.net/
[22] European Commission, Joint Research Centre, "SIML, B: An EC tool for uncertainty and sensitivity analysis," (n.d.). [Online]. Available: https://web.jrc.ec.europa.eu/rapps/pub/simlab/
[23] Chair of Risk, Safety and Uncertainty Quantification, ETH Zurich, "UQLab: The framework for uncertainty quantification," 2020. [Online]. Available: https://www.uqlab.com/

JAQUELINE CABAÑAS RAMOS received the M.Sc. degree in electrical power engineering from The University of Edinburgh, Edinburgh, U.K., in 2020. She is currently working toward the Ph.D. degree with the Institute for Automation of Complex Power Systems, E.ON Energy Research Center, RWTH Aachen University, Aachen, Germany. She is also a Research Associate with the Institute for Automation of Complex Power Systems, E.ON Energy Research Center, RWTH Aachen University. Her research interests include protection and control of DC power systems, interaction studies in MVDC system, and power electronics-based power systems.

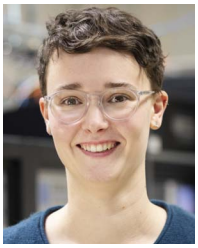

ILKA JAHN (Member, IEEE) received the Ph.D. degree in electrical engineering from the KTH Royal Institute of Technology, Stockholm, Sweden, in 2021. From 2022 to 2024, she was a Junior Research Group Leader with the Institute for Automation of Complex Power Systems, RWTH Aachen University, Aachen, Germany. In 2024, she has been an Assistant Professor with the KTH Royal Institute of Technology. Her research interests include the control and protection of HVdc systems, power systems dominated by power electronic converters, and innovative software solutions.

FERDINANDA PONCI (Senior Member, IEEE) received the Ph.D. degree in electrical engineering from the Politecnico di Milano, Milan, Italy, in 2002. In 2003, she joined the Department of Electrical Engineering, University of South Carolina, Columbia, SC, USA, where she was tenured and promoted. In 2009, she joined the E.ON Research Center, Institute for Automation of Complex Power Systems, RWTH Aachen University, Aachen, Germany, where she is currently a Professor of monitoring and distributed control for power systems. Her research interests include automation and the advanced monitoring of active distribution systems.

ANTONELLO MONTI (Senior Member, IEEE) received the M.Sc. degree (*summa cum laude*) and the Ph.D. in electrical engineering from Politecnico di Milano, Milan, Italy, in 1989 and 1994, respectively. In 2000, he joined the Department of Electrical Engineering of the University of South Carolina (USA) as an Associate and then Full Professor. He started his career in Ansaldo Industria and then moved in 1995 to Politecnico di Milano as Assistant Professor. Since 2008, he has been the Director of the Institute for Automation of Complex Power Systems within the E.ON Energy Research Center, RWTH Aachen University, Aachen, Germany. Since 2019, he has held a double appointment with Fraunhofer FIT, where he is currently developing the new Center for Digital Energy in Aachen.